

**Key Points:**

- Tropical cyclones deemed “short” by the dynamic height of the vortex metric are tilted versus shallow, vertically aligned vortices
- Dynamic height of the vortex increases sharply when storms become adequately aligned, which may be necessary for rapid intensification (RI)
- Post-alignment vertical growth during RI is sensitive to processes that affect vortex height and the warm core in the upper troposphere

**Correspondence to:**

A. J. DesRosiers,  
adesros@rams.colostate.edu

**Citation:**

DesRosiers, A. J., & Bell, M. M. (2024). Dynamic vortex height evolution during tropical cyclone rapid intensification.

*Journal of Geophysical Research: Atmospheres*, 129, e2024JD041710.  
<https://doi.org/10.1029/2024JD041710>

Received 3 JUN 2024

Accepted 2 DEC 2024

## Dynamic Vortex Height Evolution During Tropical Cyclone Rapid Intensification

Alexander J. DesRosiers<sup>1,2</sup>  and Michael M. Bell<sup>1,3</sup> 

<sup>1</sup>Colorado State University, Fort Collins, CO, USA, <sup>2</sup>Now at Cooperative Institute for Research in the Atmosphere, Colorado State University, Fort Collins, CO, USA, <sup>3</sup>Now at Department of Atmospheric Science, Colorado State University, Fort Collins, CO, USA

**Abstract** The vertical structure of the tropical cyclone (TC) vortex can be quantified throughout the TC life cycle via the dynamic height of the vortex (DHOV) metric, which is sensitive to the rate of decay of the tangential wind field with height. Observed storms always possessed a high DHOV value prior to periods of rapid intensification (RI). When limited to vertically-aligned TCs where the low- to mid-level vortex tilt magnitude is small, all DHOV values are found to be large enough for RI. Vortex tilt results from environmental vertical wind shear (VWS) and a similar relationship is found in an ensemble of TCs simulated in a moderate shear environment. Once vortex tilt decreases, both the observed and ensemble TCs exhibit a concurrent increase of DHOV and intensity, indicating the metric provides useful information about changing vertical structure in both tilted and aligned TCs. The growth of DHOV during RI is closely coupled with a strengthening warm core at the upper levels. A simulation with an upper-level jet of VWS is used to better understand the importance of the upper levels during RI by disrupting vortex development there. DHOV and intensity of the TC are effectively capped in the jet simulation relative to its counterpart in a control simulation, indicating shear can limit TC height without appreciable low- to mid-level tilt. Differences in kinematic and thermal structure between the jet and control runs are found from 12- to 16-km altitude, suggesting the importance of warming near the tropopause in powerful TCs.

**Plain Language Summary** Changes in the vertical structure of the tropical cyclone (TC) wind field are important during rapid intensification (RI). Vertical wind shear (VWS), or the changes in the magnitude and direction of environmental winds with height, can tilt the TC with respect to height and cause winds averaged around the TC center to decay rapidly with height. When tilt is minimized in a TC, the winds are strong enough at higher levels to facilitate RI. During RI, the wind field continues to expand vertically and the resulting decreased decay with height depends on warming in the upper levels of the troposphere. A metric for vertical structure evaluated in observations and numerical models in this study changes in response to both the tilting of the vortex and its aligned vertical growth. Continued study of TC vertical structure is helpful in understanding how TCs grow strong and how strong they can become.

### 1. Introduction

Tropical cyclones (TCs) are organized convective storms capable of producing vortical circulations throughout the troposphere in their most intense states. Airborne radar analyses of category-5 Hurricane Patricia (2015) offer evidence of this extreme by showing a tangential wind field spanning the full depth of the troposphere (Martinez et al., 2019; Rogers et al., 2017). TCs at powerful intensities like Patricia are massive atmospheric phenomena which generate a large area of associated hazards; however, our understanding of the processes by which these storms attain great intensity, especially when occurring quickly, is a work in progress. Successful prediction of rapid intensification (RI), or the increase in the maximum sustained winds of a TC of at least 30 kt over a 24-hr period (Kaplan & DeMaria, 2003; Kaplan et al., 2010), is historically shown to be difficult (Trabing & Bell, 2020). This is due in part to internal processes, which are hard to observe remotely, being an important contributor to RI in otherwise favorable environments capable of supporting TC intensification (Hendricks et al., 2010). TC intensity forecasts are improving relative to past performance (Cangialosi et al., 2020) indicating encouraging progress in our ability to predict rapid intensity changes. Research focused on internal processes that drive TC intensity change are important to continued intensity forecast improvement. Much of this past work explores aspects of vortex structure, with radial and azimuthal structure receiving the bulk of the attention in

comparison to the vertical structure of the TC vortex, about which there is still much to learn (X. Chen et al., 2023).

DesRosiers et al. (2023), henceforth referred to as D23, evaluated TC vertical structure in a large data set of kinematic analyses generated from tail Doppler radar (TDR) data collected during TC reconnaissance flights (Fischer et al., 2022). The study evaluated different quantities to determine the height of the vortex (HOV) and the relationships these quantities have with current TC intensity as well as intensity change. A quantity termed dynamic HOV (DHOV), defined as the height at which the maximum winds in the azimuthally-averaged tangential wind field decay to 40% of the maximum at 2-km altitude in each analysis, demonstrated a relationship with intensity change. Grouping DHOV values into intensity change groups defined by changes in minimum surface pressure ( $P_{\min}$ ) over the 24-hr period following observation revealed that a tall vertical vortex structure was always present in storms preceding periods meeting a pressure-based RI definition. The observed relationship between DHOV and intensity change is intriguing, but the physical nature of this relationship is yet to be explored. Previous observational (Fitzpatrick, 1995) and modeling (Peng & Fang, 2021) studies suggest that TCs with tall tangential wind fields are more likely to intensify at greater rates. TC vertical structure should be important during intensity change as  $P_{\min}$  is hydrostatically linked to geopotential height falls aloft in a strengthening TC. However, prior observational analysis which evaluated vertical vortex structure using the decay of tangential winds normalized to the 2-km maximum did not report an observed relationship similar to that of D23 (Stern et al., 2014; Stern & Nolan, 2011). These studies were limited to 8-km altitude and below by an older data set preceding upgrades to the sensitivity of the TDR (Aircraft Operations Center, 2016), which allowed for improved TC observation in the upper levels of the atmosphere in the data set utilized in D23.

Further study of the impact of environmental vertical wind shear (VWS), which is a change in magnitude and direction of environmental winds with height, on TC intensity is necessary to better understand the TC intensification process (Rios-Berrios et al., 2024). A relationship between VWS and DHOV is noted in D23. Large ( $\geq 10$  km), or “tall,” DHOV values are favored in lower VWS environments while small ( $< 10$  km), or “short,” values are more common when VWS is higher. VWS acts to tilt the vortex downshear, causing the low- and mid-level circulations to become vertically misaligned (DeMaria, 1996). Vortex tilt resulting from VWS can inhibit intensification until vertical realignment of the circulation occurs (Rios-Berrios et al., 2018). A tilted, asymmetric vortex struggles to project strong tangential winds in the azimuthal average taken about a fixed low-level storm center during the determination of DHOV. Therefore, smaller DHOV values may not be “short” TCs, but rather vortices tilted by environmental VWS. “Tall” DHOV values necessary for RI in D23 may be indicative of vertically aligned TCs. However, DHOV is not exclusively determined by the status of vortex alignment. The tangential wind field of the vortex continues to grow vertically during aligned TC intensification. The vertical growth process was characterized in TDR observations of the RI of Hurricane Michael (2018) as both a dynamic and thermodynamic process (DesRosiers et al., 2022). Strengthening upper-level rotation increased the DHOV and was coupled, via thermal wind balance, with a developing upper-level warm core as  $P_{\min}$  decreased in the intensifying TC.

Upper-level warm core development in TCs is not solely a tropospheric process. During the record-setting RI of Hurricane Patricia (2015), a warm core developed at the interface between the upper-troposphere and lower-stratosphere (UTLS), evidenced by novel in-situ upper-level observations (Duran & Molinari, 2018). Numerical model simulations indicate a key contributing factor of UTLS warm-core development is descent of warm stratospheric air into the eye (Ohno & Satoh, 2015). The descent is a response to diabatic heating from deep convection accompanied by growing inertial stability from the strengthening cyclonic circulation capable of trapping the heating locally (H. Chen & Zhang, 2013). The DHOV metric introduced in D23, and employed again here, can bridge the gap as a continuous vertical structure diagnostic which is informative during the earlier, tilt-susceptible TC development phase and the aligned vortex intensification phase in a continuous fashion. Investigation of changes in DHOV throughout the TC lifecycle in observations and numerical model simulations can help bolster our understanding of vertical vortex structure and its relationship to TC intensity change.

The analysis presented herein aims to further discern the physical meaning of the DHOV metric. In Section 2, observational data helps characterize the relationship between DHOV and VWS-induced vortex tilt with greater detail. Section 3 calculates and tracks the evolution of DHOV within an ensemble of simulated TCs evolving in the presence of VWS. Section 4 describes differences in DHOV and intensity in simulated TCs in a control and test simulation, in which a concentrated jet of upper-level VWS limits upper-level vortex development. Section 5

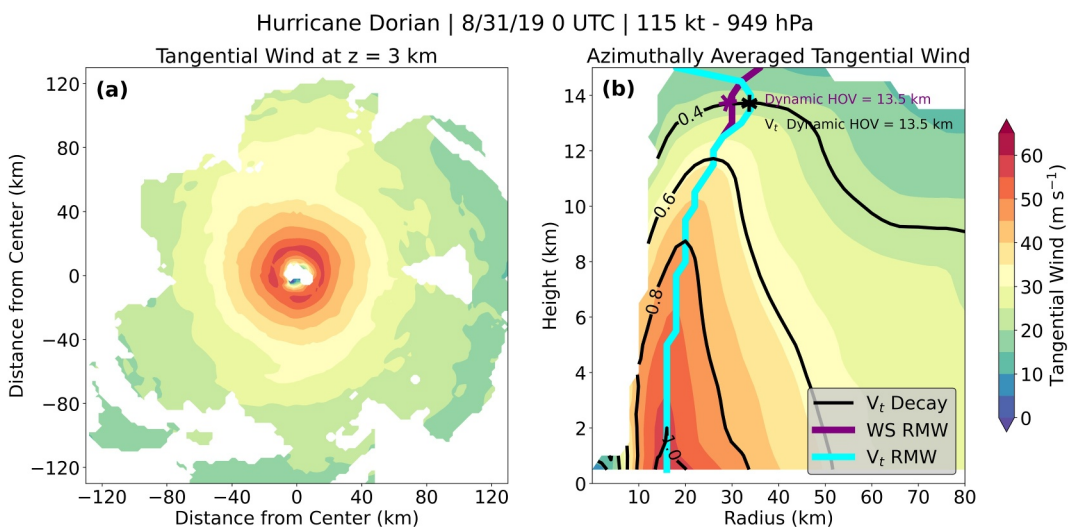


**Figure 1.** (a) Merged tangential wind analysis at a height of ( $z$ ) of 3 km from TC-RADAR in Hurricane Dorian at category-4 intensity and (b) the azimuthally-averaged tangential wind field. The radius of maximum winds (RMW) is denoted by a purple contour and cyan contour when defined by total wind speed (WS) and tangential wind ( $V_t$ ), respectively. Black contours are  $V_t$  divided by the maximum value of  $V_t$ , found at the RMW at  $z$  of 2 km. The dynamic HOV values are given for each RMW determination (asterisks; b).

discusses the findings of this study and how they relate to existing literature. Conclusions are summarized in Section 6.

## 2. Observed Relationship Between DHOV and Vortex Tilt

The DHOV analysis generated in D23, using the Tropical Cyclone Radar Archive of Doppler Analyses with Recentering (TC-RADAR) data set (Fischer et al., 2022), is revisited with an updated version of TC-RADAR (v3k) to gain greater insight into the relationship between DHOV and vortex tilt induced by environmental VWS. The merged TC-RADAR kinematic analyses are created using TDR data from aircraft reconnaissance missions into storms in the northern Atlantic and eastern and central north Pacific basins. The calculation of DHOV in TC-RADAR is illustrated with an analysis of Hurricane Dorian (2019). Merged tangential wind analyses in TC-RADAR are converted from Cartesian (Figure 1a) to cylindrical coordinates and the resulting cylindrical field is azimuthally averaged and normalized to its maximum value at 2-km altitude (Figure 1b). DHOV is defined as the height at which the azimuthally-averaged tangential wind at the radius of maximum wind (RMW) decays to 40% of its maximum value at 2-km altitude. Calculation of DHOV is mostly consistent with the methodology described in D23, however, the RMW is now defined using the tangential wind field (cyan contour; Figure 1b) rather than the full wind speed field composed of meridional and zonal components of flow (purple contour; Figure 1b). The resulting DHOV values using the tangential-wind-defined RMW are largely similar to the wind-speed-defined RMW DHOV values, with those in the Dorian sample case (asterisks; Figure 1b) being identical. The relationship between intensity change and DHOV was present in D23 using either RMW definition, but the wind speed field definition was favored in that study given a slight increase in the statistical significance of the relationship. In the current study, DHOV calculations with the prior RMW definition in model simulations were found to be sensitive to stronger radial outflow in the clear air of the eye which would not be detected in the radar observations due to the lack of scatterers in clear air. The clear air radial wind produces RMWs which can fall within the inner edge of the eyewall and lead to some undesirable sensitivity in the calculation of DHOV. To avoid this issue, the DHOV calculation now uses the RMW based on tangential wind.

Observed vortex tilt values corresponding to each case are also calculated between 2- and 6-km altitude using the vertical profiles of tilt magnitude available in TC-RADAR generated by Fischer et al. (2022). An accurate measurement of DHOV in TC-RADAR is only retained for analysis in cases with  $P_{\min}$  less than 1,000 hPa, distance to land greater than 50 km, and sufficient time over water to determine a 24-hr intensification rate following analysis. We first investigate the direct relationship between DHOV and vortex tilt shown in Figure 2.

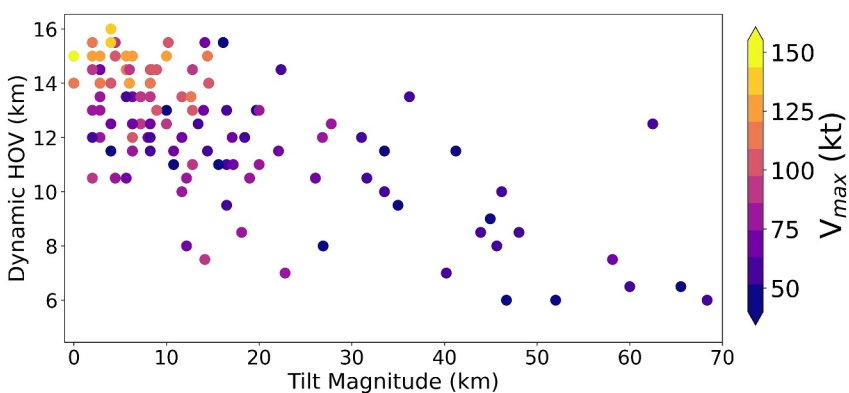
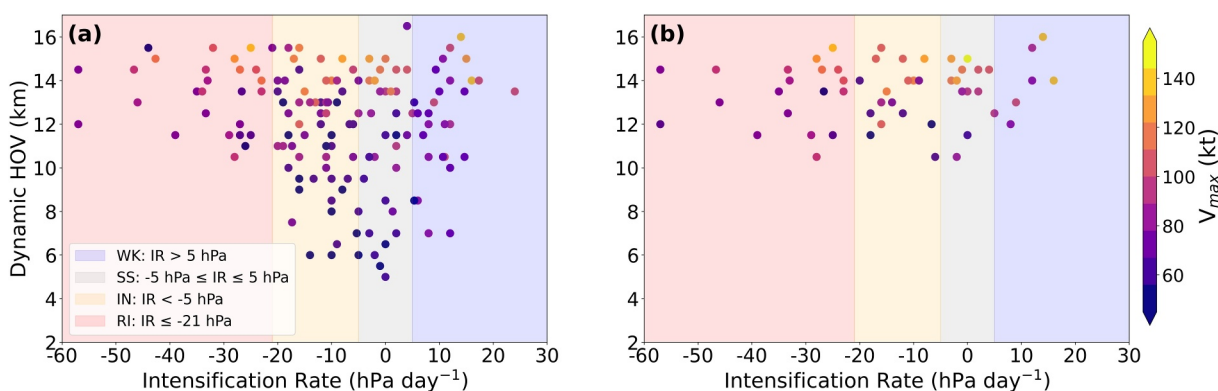


**Figure 2.** Observed dynamic HOV values in TC-RADAR versus their corresponding vortex tilt magnitudes between 2- and 6-km heights. The intensity (colorbar) is given as the maximum sustained wind ( $V_{\max}$ ) at analysis time.

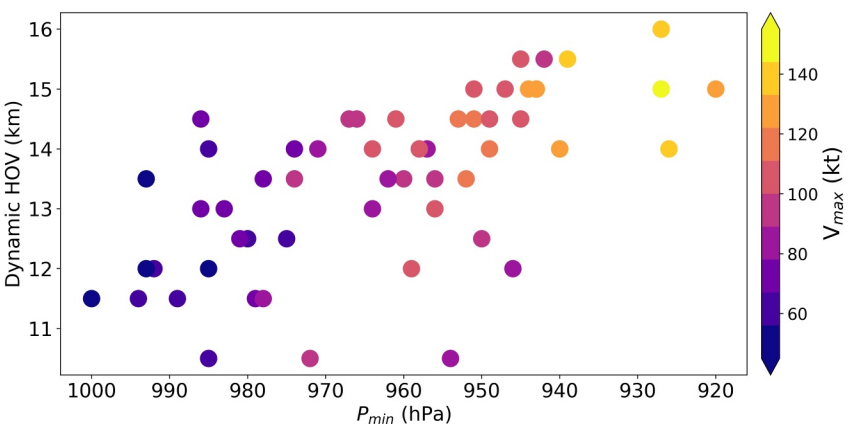
Three outlier cases with tilt  $>150$  km and DHOV  $\leq 6$  km are omitted in the figure to better display the variance in the bulk of the observed cases. There is a negative relationship in which larger tilt values correspond to lower DHOV values. A relationship between tilt, DHOV, and intensity is also evident, with storms having higher DHOV and smaller tilt magnitudes generally being more intense.

Figure 3a shows the distribution of DHOV as a function of intensity change and current intensity (colorbar). As in D23, intensity change groups are determined by 24-hr rate of change in  $P_{\min}$  following analysis time. RI is defined here as a drop in  $P_{\min}$  greater than or equal to 21 hPa, while strengthening storms that do not meet the RI threshold are in the intensifying (IN) group, and changes in  $P_{\min}$  from  $-5$  hPa to  $+5$  hPa classify as steady-state (SS). Increases in pressure greater than 5 hPa qualify for the weakening (WK) group. The distribution of DHOV values narrows toward exclusively high values ( $\geq 10$  km) in the RI group, similar to the results shown in D23. Defining aligned vortices as those with tilt magnitudes  $<10$  km and retaining only that subset of the cases shows that all observed aligned TCs exhibit DHOV values of 10 km altitude or greater (Figure 3b). The relationship between DHOV and RI discovered in D23 is no longer present, since all values are equal to or exceed the lower bound of the RI group. The result of restricting the sample to aligned vortices is consistent with alignment being a necessary but insufficient condition for rapid intensification (Rios-Berrios et al., 2018). Another important aspect of Figure 3b is that there are no observed instances of “short,” defined by DHOV values  $<10$  km, TCs in aligned storms. TCs deemed “short” by the DHOV metric were all vertically misaligned between their low- and mid-level circulation centers rather than being shallow, aligned vortices.

The color shading of the dots in Figure 3b indicates there is a positive relationship between intensity and the DHOV axis in the aligned cases. The general relationship is more evident when the DHOV of aligned cases is plotted against intensity (Figure 4). There is more spread of DHOV values in weaker storms, but as TCs approach



**Figure 3.** Dynamic HOV as a function of 24-hr intensity change rate. Intensity of storm at analysis time (colorbar) and intensity change groups (shaded) are shown with intensification rate (IR) bounds for groups given (legend). Dynamic HOV defined by tangential wind RMW is shown for (a) all cases and (b) aligned cases with vortex tilt magnitudes less than 10 km.



**Figure 4.** Dynamic HOV as a function of storm intensity, evaluated with  $P_{\min}$ . Wind-based intensity of storms at analysis time is shaded for each case plotted (colorbar).

and attain major hurricane intensity (Category 3+;  $P_{\min} \leq 960$  hPa), as defined by the pressure-based intensity scale proposed by Klotzbach et al. (2022), the upward trend indicates continued vertical growth of the vortex. The most intense TCs have the highest DHOV values, suggesting the metric contains additional useful information about vertical structure in aligned TCs as well as tilted ones. The signal for vertical growth of the vortex during intensification seen here is consistent with observations in DesRosiers et al. (2022), but the further analysis with respect to tilt suggests that DHOV may mean different things depending on whether the storm is tilted or aligned. Since the observations from TC-RADAR are snapshots at different stages of the TC lifecycle in different storms, it is difficult to assess whether the changing DHOV values are indicative of a vertical alignment or vertical growth process. Further analysis with numerical models is required to improve the interpretation of the DHOV metric throughout TC intensification.

### 3. Dynamic Vortex Height Evolution in Moderate Vertical Wind Shear

A 20-member ensemble of idealized TC simulations with the Advanced Research version of Weather Research and Forecasting (ARW-WRF; version 3.1.1) model (Skamarock et al., 2008) is employed here to gain a greater understanding of the DHOV metric in TCs impacted by moderate deep-layer VWS. The ensemble was used by Tao and Zhang (2014) and Nam et al. (2023) as part of a larger set of simulations with varying VWS magnitudes, sea surface temperatures (SSTs), and atmospheric moisture profiles. The 20-members used herein are from the SH7.5/Moist100 ensemble in Nam et al. (2023). Simulations are initialized with a modified Rankine vortex profile with a  $15 \text{ m s}^{-1}$  tangential wind maximum at 135-km radius. The tangential winds of the initialized vortices decay to  $0 \text{ m s}^{-1}$  at 15-km altitude. Figure 5 shows the VWS profile that would be classified as moderate ( $7.5 \text{ m s}^{-1}$ ) by the climatology described in Rios-Berrios and Torn (2017), introduced via the point downscaling method from Nolan (2011). The thermodynamic profile is initialized using the non-Saharan air layer mean hurricane season sounding (Dunion & Marron, 2008) and  $29^\circ \text{C}$  SSTs. Random perturbations are added to the boundary layer moisture to generate the 20-members. The simulations use the WRF single-moment 6-class microphysics (WSM6) scheme (Hong et al., 2004), Yonsei University (YSU) boundary layer scheme (Hong et al., 2006), and no radiation scheme or cumulus parameterization. There are 41 vertical levels with a model top at 20-km altitude. Three two-way nested domains have horizontal resolutions of 18, 6, and 2 km, with the innermost domain analyzed in this study being  $720 \text{ km} \times 720 \text{ km}$  with  $360 \times 360$  grid points. This innermost domain is centered on the vortex center at the 850 hPa level. The simulated TCs are integrated forward in a domain set on a doubly periodic f-plane at  $20^\circ \text{N}$  for 9 days. See Tao and Zhang (2014) and Nam et al. (2023) for additional ensemble simulation details.

All variables were interpolated to height coordinates from WRF sigma levels with 400-m spacing between interpolated levels. Vortex tilt calculations between roughly 1- to 6-km altitude performed by Nam et al. (2023) are used for time series analysis of the ensemble set. Note that “roughly” and “approximately” when used with respect to altitudes and radial locations in model simulation discussions indicate that the closest interpolated

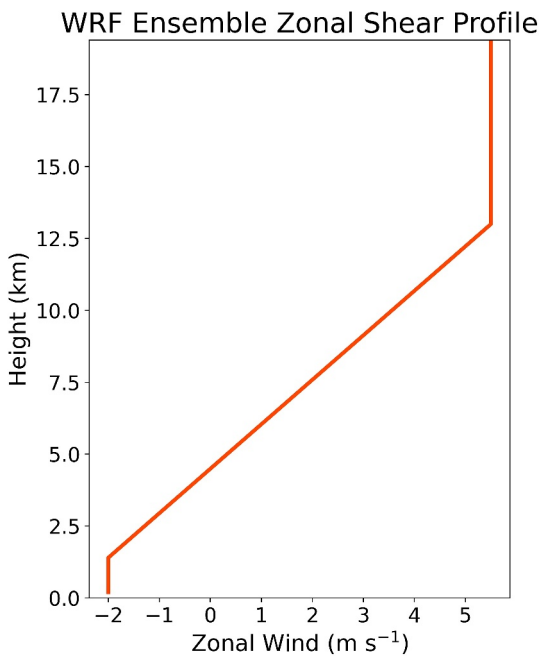


**Figure 5.** Prescribed moderate environmental zonal wind shear in the WRF ensemble simulations.

location to this point has been used in its place. Results are invariant to the choice of an interpolated coordinate above or below the approximate point so the behavior neighboring these layers is consistent. Vertically interpolated zonal and meridional winds are transformed into a tangential wind field in the innermost storm-following domain. The tangential winds are azimuthally averaged with a tangential-wind-defined RMW used to calculate DHOV at each model time step consistent with the process for the TC-RADAR analyses.

The 20-member WRF ensemble allows for analysis of the evolution of DHOV and other storm metrics with greater temporal resolution than the observations. All members experience initial vortex tilt induced by the VWS followed by alignment and RI with varied timing (Figures 6a and 6c). A time series of DHOV values is shown in Figure 6b to characterize the vertical structure of the vortex. Initially, DHOV values are predominantly below 8 km and vortex tilt values are mostly greater than 100 km with substantial variability. As the vortex comes into alignment in each member, there is a large jump, or sharp increase, in DHOV. The hour at which DHOV jumps to higher values which equal or exceed 10 km and maintains higher values for all subsequent model time steps is considered here to be the time of alignment, which corresponds to an average tilt of about 50 km. For efficient comparison of all ensemble members, the time series for all members are shifted with respect to this time, which is set to hour 0. The shifted time series are shown in Figures 6d–6f and reveal a similar temporal evolution of  $P_{\min}$ , DHOV, and tilt across all members.

Three distinct phases in the DHOV are apparent that are shaded in green, yellow, and red backgrounds and correspond to pre-alignment, a period of active alignment, and post-alignment vertical growth. The pre-alignment phase prior to the DHOV jump is characterized by slowly falling  $P_{\min}$  (Figure 6d), low and sometimes erratic

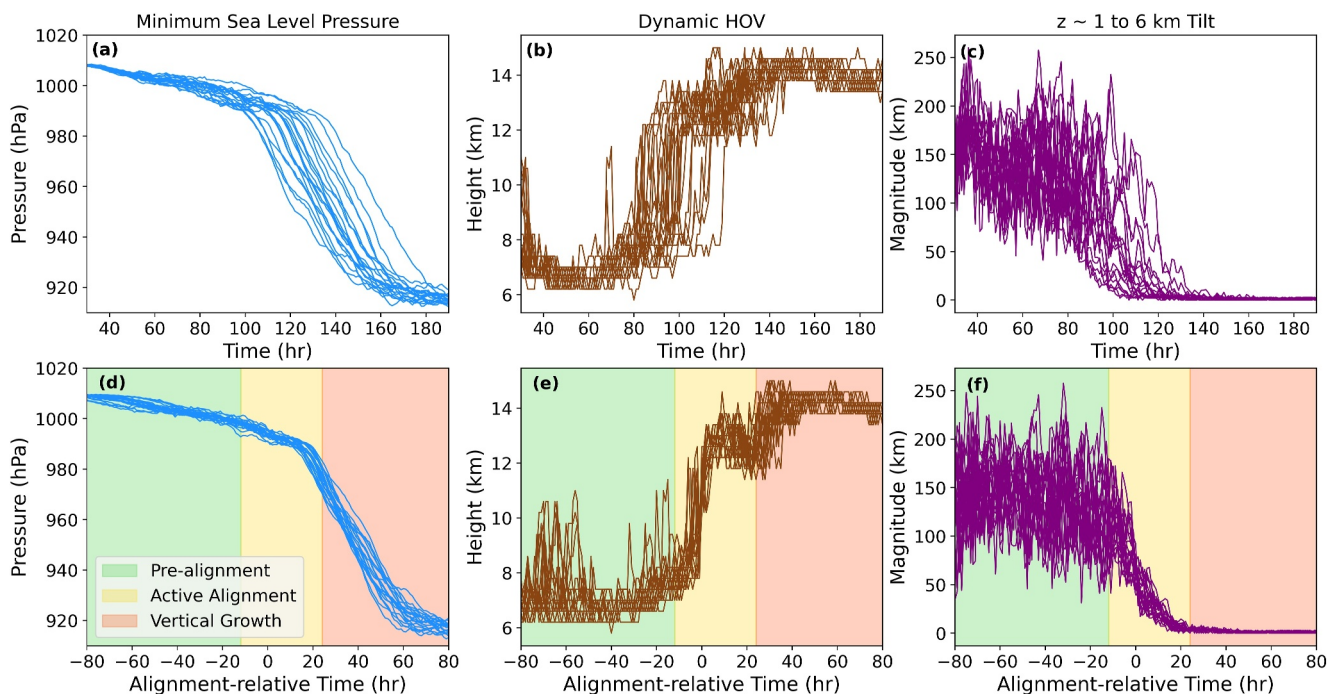


**Figure 6.** Evolution of all 20 WRF ensemble members. The (a)  $P_{\min}$ , (b) Dynamic HOV values, and (c) height ( $z$ ) of 1–6 km vortex tilt values are given as time series in the original model time. The same variables are given with the time now centered on time of alignment (d, e, f). Shading denotes the time periods of the pre-alignment (green; −80 to −12 hr), active alignment (yellow; −12 to +24 hr), and vertical growth (+24 to +80 hr) stages of intensification.

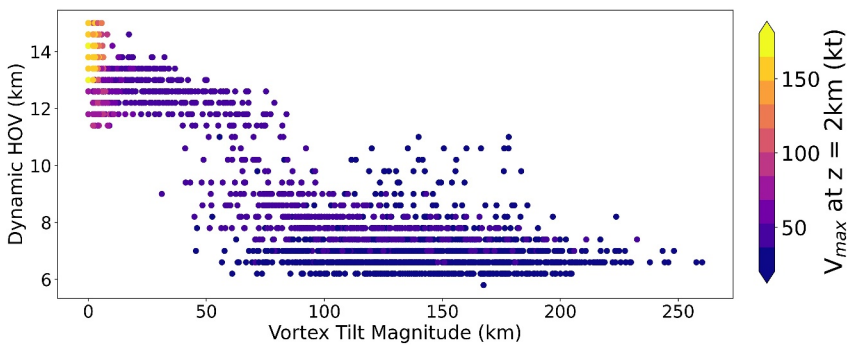


**Figure 7.** DHOV at all times across all members of the WRF ensemble simulations versus their corresponding vortex tilt magnitudes between roughly 1- and 6-km heights. The intensity (colorbar) is estimated via the maximum value of azimuthally averaged tangential wind at a height ( $z$ ) of 2 km.

DHOV values (Figure 6e), and large vortex tilt (Figure 6f). During active alignment, the pressure continues to slowly fall and the tilt steadily decreases. As the tilt declines, the DHOV values show a jump followed by a drop to a minimum height near 12 km (Figure 6e). Following the relative minimum in DHOV, the vortex height then grows toward a maximum near or above 14-km altitude. We denote that relative minimum as the start of the post-alignment vertical growth phase which occurs shortly after the onset of RI with rapidly falling  $P_{\min}$  (Figure 6d) and tilt magnitudes near zero (Figure 6f).

The relationship between DHOV and tilt across the WRF ensemble is shown in Figure 7. A wind-related intensity (colorbar) is given as the maximum azimuthally-averaged tangential wind value at 2-km height. A relationship similar to that of the TC-RADAR observations is seen, with lower DHOV associated with higher tilts. The distribution in the ensemble is approximately bimodal, with two distinct clusters of DHOV above and below 10 km associated with small and large tilt. DHOV values below 10 km are associated with tilts greater than 50 km and weaker intensities. The first 12 hr of model time in each member is excluded to remove outliers with no tilt and low DHOV associated with the model initialization time where the simulated vortices have yet to be impacted by the VWS. DHOV values above 10 km show a relationship with tilt and intensity similar to the observations, with the strongest storms having the smallest tilt. The presence of larger tilt values here as compared to the observed samples (Figure 2) is due in part to coverage limitations of airborne radar which may struggle to capture the entire wind field of a TC with high magnitude vortex tilt. The distribution of DHOV values provides further evidence that 10 km is a reasonable demarcation between misaligned and vertically aligned storms.

Since all members undergo a similar evolution in this idealized simulation, a representative member with near average values of the ensemble is selected to illustrate the changes in vertical structure in the simulated TCs (Figure 8). In addition to the prior metrics, the maximum tangential wind velocity near 2-km height (Figure 8b) and upper-level temperature perturbation (Figure 8e) are tracked as time series. The latter quantity is an average of the perturbation temperatures between 12- and 16-km altitude within the radial location of the RMW at 2-km altitude. The perturbation is in reference to the azimuthally-averaged temperature profile at roughly 300-km radius, well away from the TC center. The low-level tangential wind increases slowly during the pre-alignment and active alignment phases, while the upper-level temperature perturbation changes very little. Just past alignment-relative hour +10, the 2-km tangential winds begin to increase quickly and the pressure falls rapidly signaling the onset of RI. Shortly after RI onset near the +20 alignment-relative hour, the upper-level warm core perturbation temperature begins to increase rapidly in all members.

The azimuthally-averaged vertical structure of perturbation temperatures and tangential winds at specific times of interest (gray dashed lines) are shown for the representative member in Figures 8f–8j. At alignment-relative model hour  $-30$ , the tangential wind field is weak and concentrated in the lower levels (Figure 8f) resulting in low DHOV. The TC warm core temperature perturbation is concentrated below 6-km altitude at this time. At alignment hour 0, the tangential wind field appears somewhat disorganized, but has greater coverage with respect to height (Figure 8g), which nearly doubles the DHOV from hour  $-30$ . The warm core temperature perturbation is stronger, but remains concentrated in the lower-troposphere. 10 hours after alignment time, the tangential wind field appears more organized (Figure 8h), although the maximum value is only slightly higher than at hour 0.

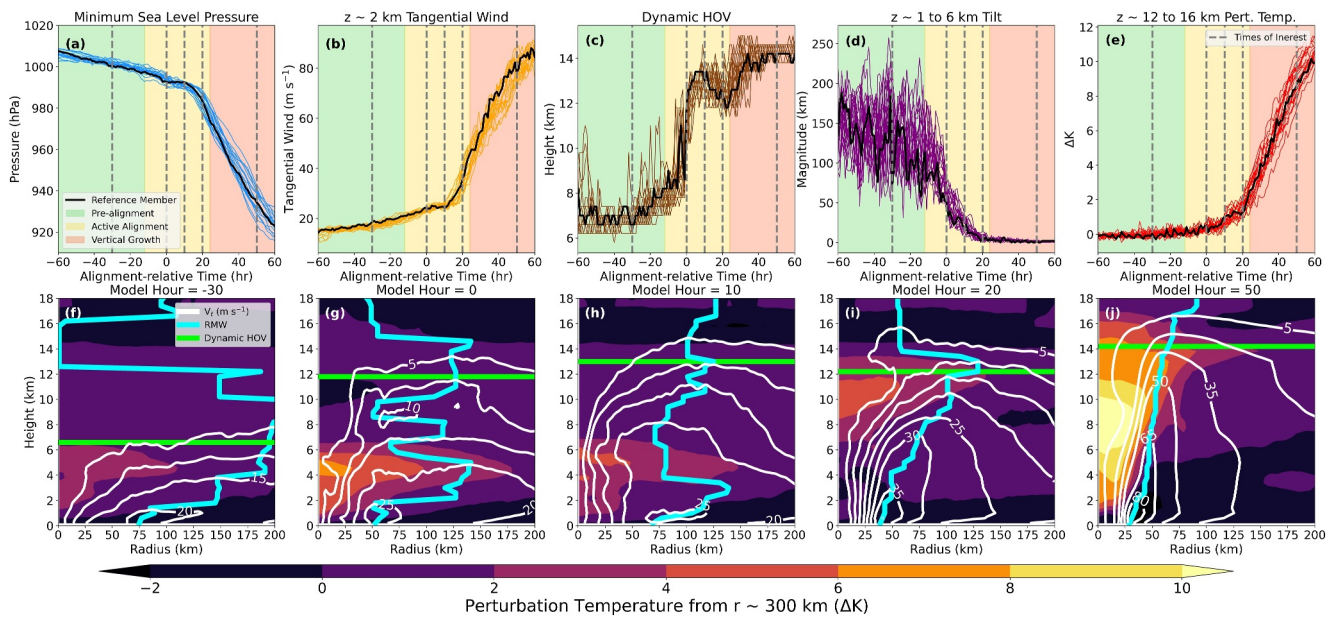


**Figure 8.** Time series plots for all members showing (a)  $P_{\min}$ , (b) maximum azimuthally-averaged tangential wind at altitude ( $z$ ) of 2 km, (c) dynamic HOV, (d) magnitude of  $\sim 1$ –6 km vortex tilt, and (e) averaged perturbation temperature from approximately 12- to 16-km height within the RMW at approximately 2-km height. The phases of intensification are indicated by background shading (legend). A representative member (black line; a–e) is highlighted with the temperature perturbation (colorbar) shown with respect to an azimuthally-averaged reference profile at radius ( $r$ ) of roughly 300 km and tangential winds (white contours) given at several times of interest (gray dashed lines; a, b, c, d, e). The RMW and DHOV are denoted at each reference time by cyan and green lines, respectively. The times of interest are alignment-relative model hours (f)  $-30$ , (g)  $0$ , (h)  $10$ , (i)  $20$ , and (j)  $50$ .

Dynamic HOV increased slightly, but the strongest temperature perturbation remains in the lower troposphere and has become more diffuse with a weaker maximum. Between model hours 10 and 20, the DHOV decreases slightly following its jump and there is a noticeable change in the thermal structure of the TC warm core. The near-surface tangential winds become more intense and the maximum of the temperature perturbation is centered near 10-km altitude (Figure 8i). The slightly decreased DHOV is just above the warm-core perturbation temperature maximum at this time, which is likely related to an increase in the DHOV-determining threshold value and adjustments with respect to thermal wind balance between the developing warm-core maximum and tangential wind field. By hour 50, RI is nearly complete and DHOV remains steady at its maximum. The tangential wind field is considerably larger in both magnitude and vertical extent (Figure 8j). The warm core temperature perturbation is maximized near 8-km height but remains strong up to and near the level of the DHOV value, and decays rapidly above it along with the tangential winds.

Inspection of the horizontal wind structure in the representative member at the 1- and 6-km levels at the times of interest is helpful in understanding the importance of vortex tilt to the evolution of vertical structure. At hour  $-30$ , the low level circulation is weak and asymmetric while the mid-level circulation is displaced to the east by the westerly VWS (Figures 9a and 9b). Tilt magnitude is large at this time (Figure 8d) as evidenced by the mismatch in TC center locations at each level obtained with the pressure centroid method of Nguyen et al. (2014). Winds are weak at both levels at hour 0 (Figures 9c and 9d), but the tilt is reduced and the centers are much closer. The 6-km rotational flow about the center is much better defined, explaining the jump in DHOV occurring at this time (Figure 8c). At hour 10, when DHOV reaches its initial post-alignment peak, the centers continue to move closer to one another (Figures 9e and 9f), although not yet fully aligned, and the wind field becomes more symmetric and well-defined at the 6-km level. DHOV is near its minimum in the active alignment phase during hour 20. Although the organization of the wind field has improved at both levels (Figures 9g and 9h), the most drastic improvement and intensification of the winds occurs in the lower levels, which contributes to the reduction of DHOV by increasing maximum winds at 2-km faster than the upper-level winds (Figure 8b). By the end of RI at hour 50, the wind fields at both levels are strong, well defined, and clearly vertically stacked (Figures 9i and 9j), indicating a vertical structure that maximizes the DHOV metric.

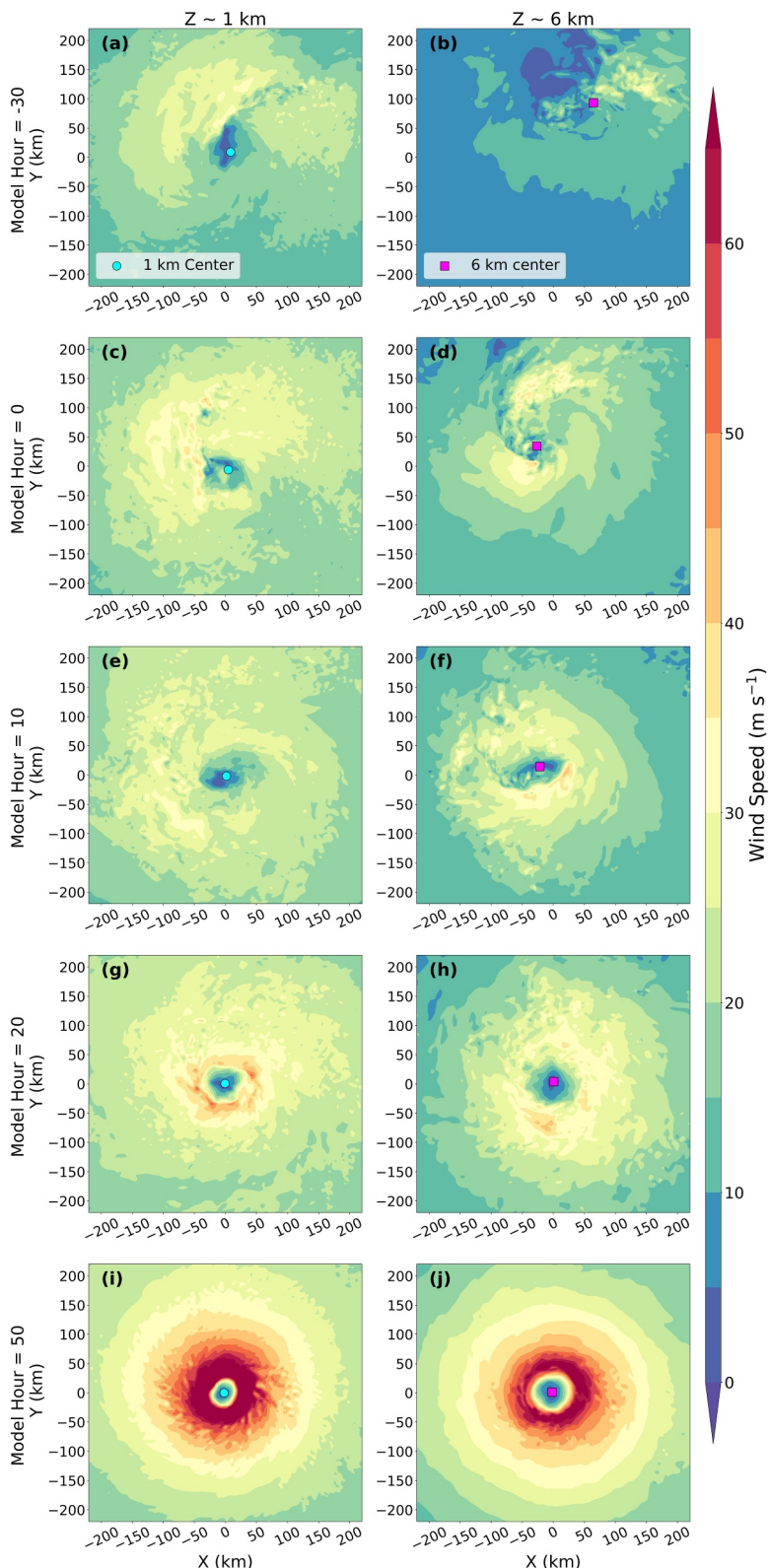


**Figure 9.** Wind speed (colorbar) given for the reference member at height ( $z$ ) of approximately 1 km at alignment-relative model hours (a)  $-30$ , (c)  $0$ , (e)  $10$ , (g)  $20$ , and (i)  $50$ . The winds near 6-km altitude are also shown for hours (b)  $-30$ , (d)  $0$ , (f)  $10$ , (h)  $20$ , and (j)  $50$ . Vortex centers are given at the  $\sim 1$ -km (cyan circles) and 6-km (magenta squares) levels.

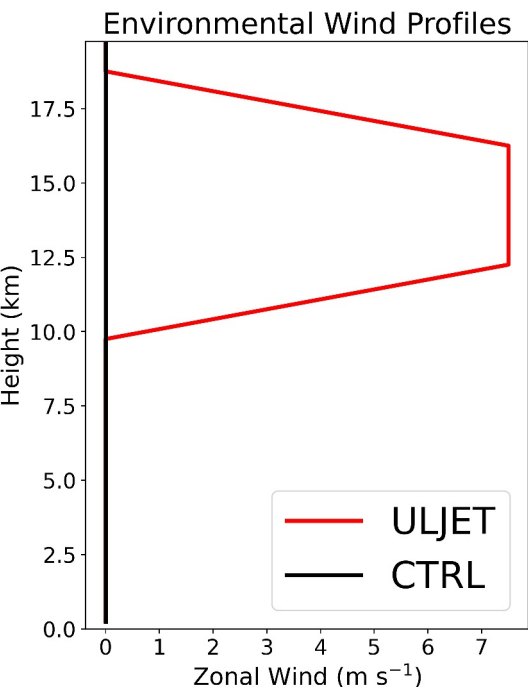


**Figure 10.** Prescribed calm environmental zonal wind profile in the control simulation (CTRL; black) and the profile of the upper-level jet (ULJET; red) simulation.

ments from the referenced study are 2-km horizontal resolution, SSTs of 29°C, and use of the Thompson microphysics scheme (Thompson et al., 2004), which has demonstrated skill in TC model forecasts (Choudhury & Das, 2017). A simple Louis-type scheme is used in the planetary boundary layer (Bryan & Rotunno, 2009) and the Rapid Radiative Transfer Model for General circulation models (RRTMG) scheme is used for shortwave and longwave radiation. The storm-following horizontal grid, which is centered on the minimum surface pressure, is composed of  $540 \times 540$  grid points and is  $2,000 \text{ km} \times 2,000 \text{ km}$  on an f-plane at 20°N. Uniform 2-km horizontal resolution is maintained over the innermost  $620 \text{ km} \times 620 \text{ km}$  and stretches outward to 10-km resolution at the domain boundaries. The vertical grid stretches from 50- to 500-m resolution from 0- to 5.5-km altitude where a uniform 500-m resolution is maintained until model top at 25 km, resulting in 59 vertical levels.

The two simulations are differentiated by their environmental VWS profiles shown in Figure 10. The control simulation, referred to as CTRL, has no background flow or VWS. The test simulation, referred to as ULJET, introduces a  $7.5 \text{ m s}^{-1}$  upper-level zonal jet via the time-varying point downscaling technique (Onderlinde & Nolan, 2017). The jet is constructed such that a bulk shear calculation returns the same VWS value of  $7.5 \text{ m s}^{-1}$  as the WRF ensemble when evaluated between the 850 to 200 hPa layer, despite the strongest zonal winds being focused in the upper levels above quiescent flow through much of the troposphere. The focused upper-level VWS in the jet is intended to affect the development of the upper-troposphere lower-stratosphere (UTLS) warm core which forms in the CTRL simulation, while having little to no impact on the alignment of the developing vortex in the lower to middle troposphere. After allowing for initial convective development in calm flow, the VWS profile is nudged in at the boundaries in ULJET from model hours 12 to 24 consistent with the methodology of Alland et al. (2021).

Results from the WRF ensemble indicate the importance of a strengthening upper-level warm core temperature perturbation to the deep vertical structure obtained by TCs during the RI process. The additional experiments run in CM1 serve as a mechanism denial experiment in which a concentrated upper-level jet of moderate VWS is used to disrupt the formation of the UTLS warm core in the ULJET simulation. The TC is allowed to develop in a similar environment over the first 12 hr, and then during hours 12–24, the upper-level jet ramps up in ULJET and is maintained from hour 24 onward. Through the first 3 days of the model simulations, RI proceeds in a qualitatively similar fashion with respect to maximum surface wind speeds (Figure 11a) and  $P_{\min}$  (Figure 11b) with the

#### 4. Dynamic Vortex Height Evolution During Rapid Intensification in the Post-Alignment Vertical Growth Phase

An additional set of numerical model experiments is devised to further explore DHOV evolution during the post-alignment vertical growth phase noted in the WRF ensemble. We hypothesize that the low to mid-level alignment is primarily disrupted by VWS in the low to mid-troposphere, and that aligned storms with VWS confined to the upper troposphere would not need to undergo the active alignment phase and could move directly into the third phase of development. We further hypothesize that the vertical growth of DHOV above 10 km is an important structural characteristic during RI. These hypotheses are tested using a pair of Cloud Model 1 (CM1; version 21.0) (Bryan & Fritsch, 2002) simulations. The change from WRF to CM1 also allows us to test the sensitivity of the conclusions regarding DHOV using a different dynamical core and physics parameterizations to ensure that the metric still provides a similar interpretation in a different modeling framework.

Both CM1 simulations are initialized with a modified Rankine vortex with maximum winds of  $15 \text{ m s}^{-1}$  located at 75-km radius from storm center, consistent with defaults for TC initialization set in the model and similar to the WRF initial vortex. The tangential winds of the initialized vortices decay to  $0 \text{ m s}^{-1}$  at 15-km altitude. The moist tropical profile in Dunion (2011) is used to initialize the thermodynamic environment, which is slightly less moist than the Dunion and Marron (2008) profile used in WRF, but qualitatively similar. The model configuration is largely similar to that described in Martinez et al. (2022). The main differences present in these CM1 experiments

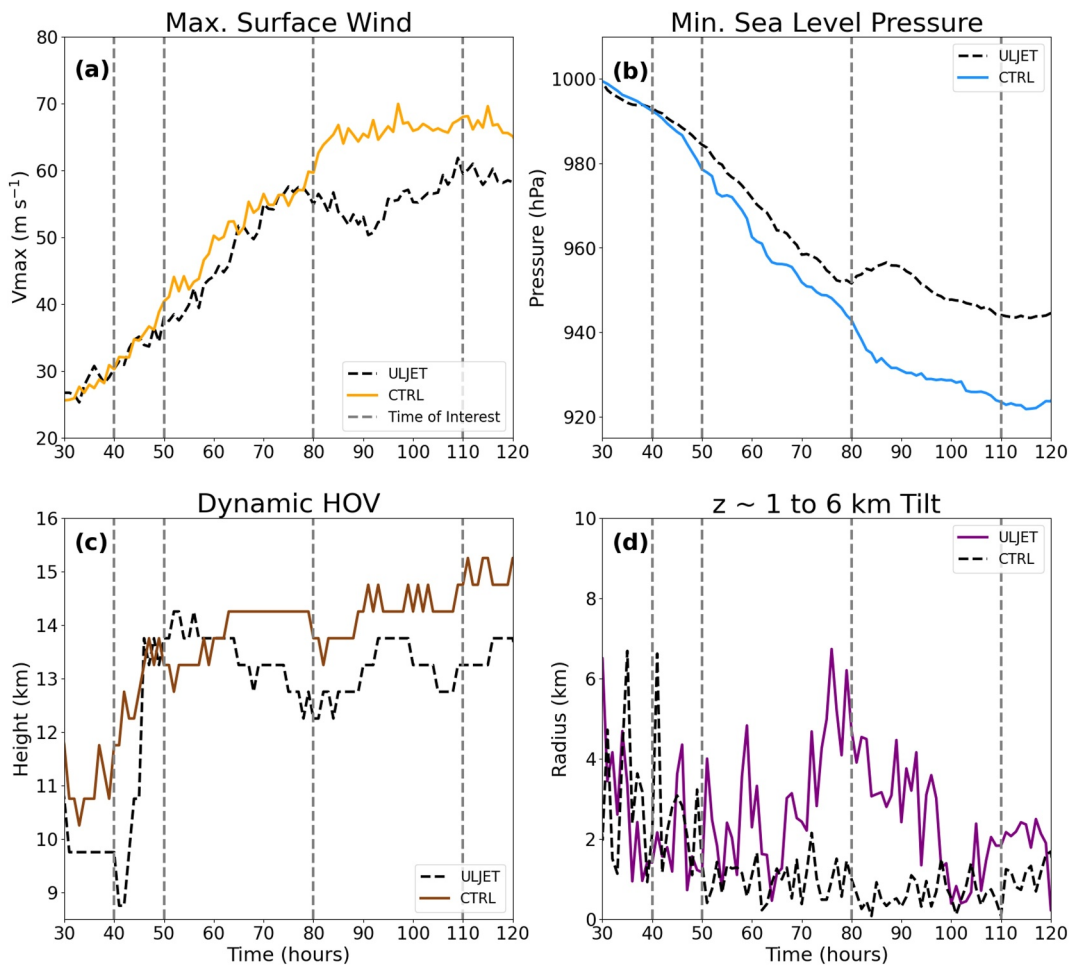


**Figure 11.** Time series of (a)  $V_{\max}$ , (b)  $P_{\min}$ , (c) dynamic HOV, and (d) approximately 1- to 6-km vortex tilt magnitude for the control run (CTRL; solid colored lines) and the upper-level jet run (ULJET; dashed black lines) with times of interest shown (gray dashed lines).

intensity of the simulated TC in ULJET lagging slightly behind CTRL. Near hour 75 and onward, the intensities begin to diverge and RI continues in CTRL while the intensity in ULJET weakens briefly. The DHOV values diverge earlier with ULJET beginning to decline around hour 60 while CTRL continues to increase the vertical extent of its tangential wind field (Figure 11c). There is also a slight increase in the zonal motion of the TC in ULJET versus that of CTRL on the order of a few  $\text{m s}^{-1}$  near hour 60 (not shown), providing evidence of the TC being impacted by the jet at this time. There is a sharp initial rise in DHOV followed by a lull in growth in CTRL, but the slight decline in DHOV seen in the WRF ensemble at the end of active alignment is not present. An alignment period is not necessary as there is no appreciable (magnitude  $\geq 10 \text{ km}$ ) tilt of the vortex in the low- to mid-troposphere where the flow is quiescent in both simulations (Figure 11d). ULJET does eventually recover from its brief weakening period and declining DHOV, but the peak TC intensity and DHOV value are noticeably lower than in CTRL. The differences between simulations suggest that the upper-level jet limits the vertical development of the TC vortex and its intensity. Since these simulations include radiation, eyewall replacement cycles (ERCs) become more likely to occur (Trabing & Bell, 2021). An ERC would temporarily weaken the TC and likely decrease the DHOV as the newly formed eyewall overtakes the primary and would need to undergo its own period of vertical growth. The RMW at 2-km altitude holds steady near 35-km radius in both simulations (not shown) over the time analyzed, confirming that ERCs did not impact the behavior of the simulated TCs, such that the differences cannot be attributed to such a mechanism.

Times of interest in Figure 11 are identified to highlight differences in the tangential wind field and warm core structure (Figure 12). The warm core structure is again evaluated through azimuthally-averaged perturbation

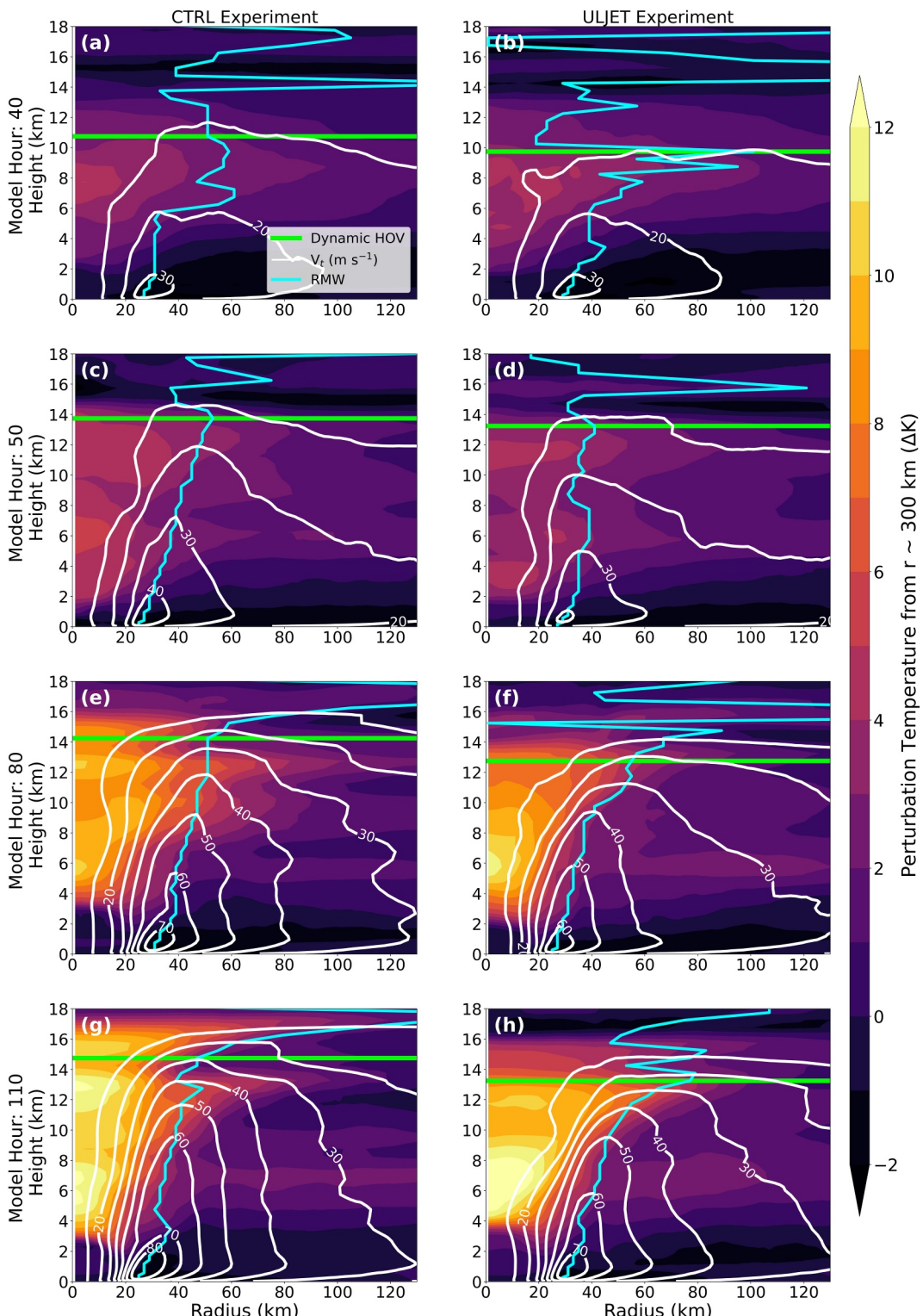


**Figure 12.** Azimuthally-averaged perturbation temperature (colorbar) from an azimuthally-averaged reference profile at radius ( $r$ ) of approximately 300 km. Analyses are shown at model hours 40, 50, 80, and 110 for the control (CTRL; a, c, e, g) and upper-level jet (ULJET; b, d, f, h) simulations. The radius of maximum winds (RMW; cyan contour), dynamic HOV (green line), and tangential winds (white contours) are shown for all times of interest.

temperatures from a 300-km radius reference profile similar to the WRF ensemble. At hour 40, the wind intensities of ULJET and CTRL are similar, but the warm core temperature perturbation is more diffuse and the tangential wind field is less vertically expansive in ULJET compared to its counterpart in CTRL (Figures 12a and 12b). At hour 50, following the initial rise in DHOV, the winds are stronger and more organized in CTRL (Figures 12c and 12d) with a steady outward slope of the RMW (cyan contour) apparent. A warm core temperature perturbation forms around 12-km altitude in both simulations, but is better defined and more expansive in CTRL. Intensity and DHOV values have diverged by hour 80 (Figure 11) and the vertical structure is different as well (Figures 12e and 12f). The warm core temperature perturbation is much weaker above 14 km in ULJET with a strong maximum forming near 6-km altitude. The maximum perturbation temperature in the eye is weaker in CTRL, but dual maxima are present near 6- and 12-km altitude. Strong cyclonic winds in the eyewall extend higher into the troposphere in CTRL. Near the peak steady-state intensity for each simulation at hour 110, the inner-core structures are quite different (Figures 12g and 12h). The RMW is more upright in CTRL and the tangential wind field is stronger with most of its decay in magnitude occurring much higher in the troposphere, resulting in a higher DHOV than ULJET. An additional warm core perturbation temperature maxima forms above 14-km altitude. With a single perturbation temperature maximum still dominant in ULJET and a warm core that decays rapidly above 14-km altitude, the wind field in ULJET decays much faster in the upper-troposphere.

To further examine the detailed evolution of vertical structure, the strength of the tangential wind field and warm core temperature perturbation are averaged in several vertical layers throughout the analyzed period of CTRL and ULJET (Figure 13). Azimuthally-averaged fields from hour 100 of CTRL are used as a visual aid for the method of averaging. At each model time step, the tangential winds are normalized to their maximum at 2-km altitude along the RMW through the 0- to 4-km, 4- to 8-km, 8- to 12-km, and 12- to 16-km levels (Figure 13a; legend). The resulting time series are given in each layer in CTRL (Figure 13c) and ULJET (Figure 13e). The perturbation temperature is averaged over the same layers within a box radially bounded by the center of the TC and the location of the 2-km RMW at each time step (Figure 13b; legend). While the warm core grows radially with height as the RMW and eyewall slope outward, the averages are bounded by the lower-level RMW to focus on its impact on the minimum central surface pressure. The time series of these averaged quantities in CTRL (Figure 13d) and ULJET (Figure 13f) allow for comparison of the developing warm core to the strengthening tangential winds at the corresponding levels. Winds in the lowest layer are unsurprisingly static near 1.0 in both simulations, since the scaling value is calculated in this layer. The warm core is largely nonexistent through the lowest layer. Later in the simulations once the intensities have diverged, the winds and temperature perturbations in the middle two levels plateau and remain mostly static with the values being slightly larger in ULJET as compared to CTRL. The similar behavior in these levels is likely due to the environmental winds being zero through the bulk of these layers in both simulations, thus allowing for intensification of the TCs in predominantly quiescent background flow.

The most noticeable differences in this analysis are found in the upper level from 12- to 16-km altitude. Following the onset of RI in both simulations, the upper-level winds and warm core intensify with the TC. The averaged winds and perturbation temperatures experience consistent growth throughout the analysis period in CTRL, with the strongest rates of increase occurring in tandem during the period of RI. Once a steady-state intensity in terms of maximum winds is reached, the average values of all quantities in the lower three levels remain static. The upper-level winds and temperature perturbation continues to grow along with DHOV as the minimum pressure drops into extreme values below 930 hPa. In ULJET, the winds and temperature perturbation increase in the upper-levels during RI. At the end of the RI period in ULJET, when the intensities of the simulated TCs diverge, the averaged values in this level begin to decline and subsequently never reach the values at peak intensity in CTRL. Accordingly, vortex development in the upper levels is capped in ULJET and the DHOV and intensity do not increase in a manner similar to CTRL. Although some metrics in the upper-levels of ULJET do increase, the difference is more stark when comparing changes from 14- to 16-km in the uppermost part of the TC circulation. The UTLS warm core which has been observed and simulated (Duran & Molinari, 2018; Ohno & Satoh, 2015) should form here, in the highest levels of the troposphere. The difference in structure becomes apparent at hour 80 when the warm core temperature perturbation continues to expand vertically and DHOV is higher in CTRL (Figures 12e and 12f). The tangential wind field is weak, but well defined in this level while the RMW remains upright and further radially inward in the middle and upper levels in CTRL. By hour 110 (Figures 12g and 12h), the additional perturbation temperature maxima is present in CTRL and absent in ULJET.

Although deciphering relationships between vortex height and intensity change requires more attention be paid to the upper levels of the atmosphere, the evolution of this layer alone paints an incomplete picture. As noted by

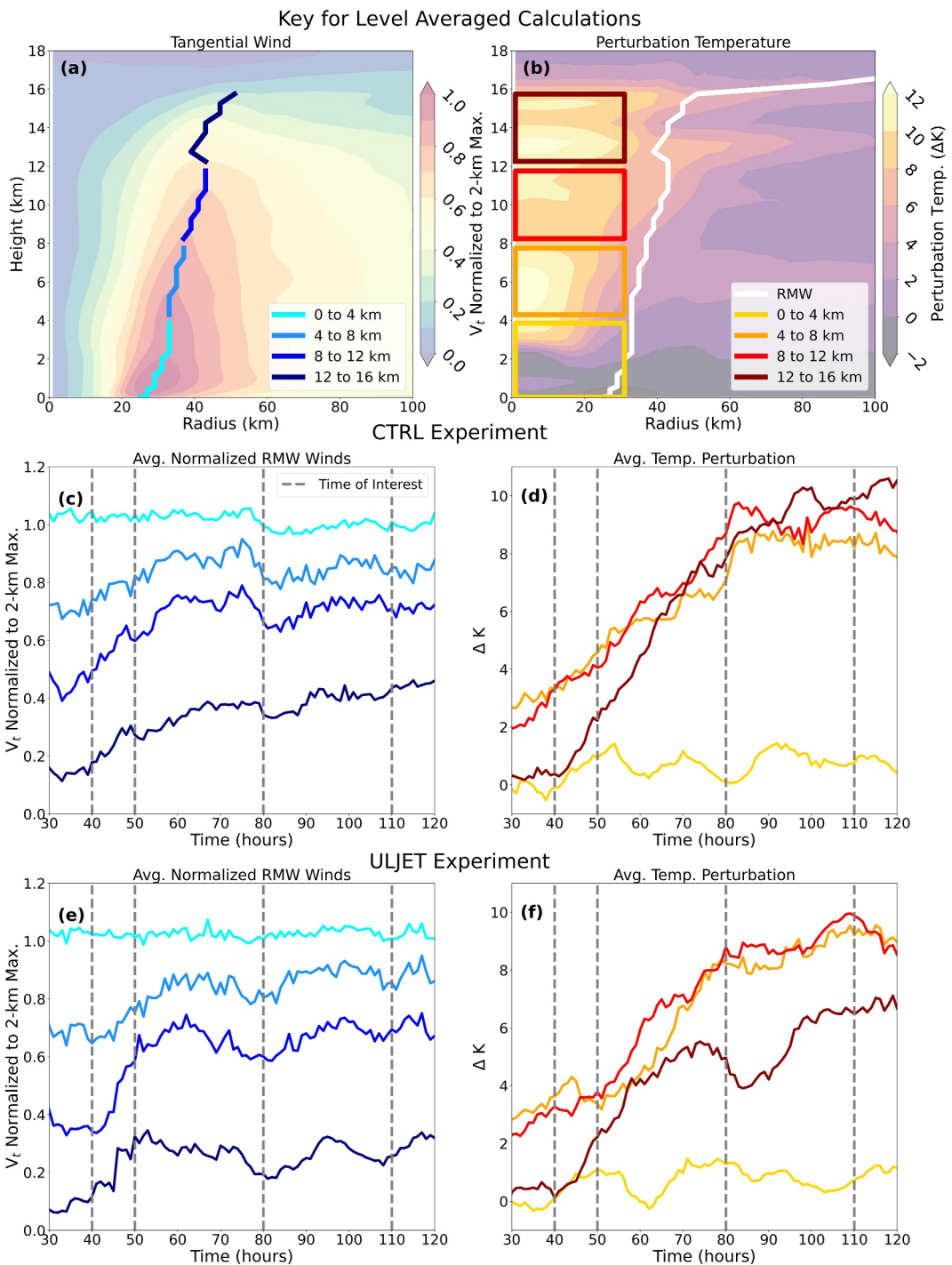


**Figure 13.** (a) Azimuthally-averaged profile of tangential winds normalized to the maximum at height ( $z$ ) of 2 km (colorbar; a) at model hour 100 in the control (CTRL) simulation normalized to the 2-km maximum. Colored lines denote the tangential wind values averaged over specific levels (legend; a). Averaged wind values are given as time series for the (c) CTRL and (e) upper-level jet (ULJET) simulations. (b) Azimuthally-averaged profile of perturbation temperature (colorbar; b) with respect to an azimuthally-averaged reference profile at radius ( $r$ ) of roughly 300 km. The radius of maximum winds (RMW) is shown as a white line. Averaged temperature values over specific levels (legend; b) are given as time series for the CTRL (d) and ULJET (f) simulations. Times of interest are given as dashed gray lines (c, d, e, f).

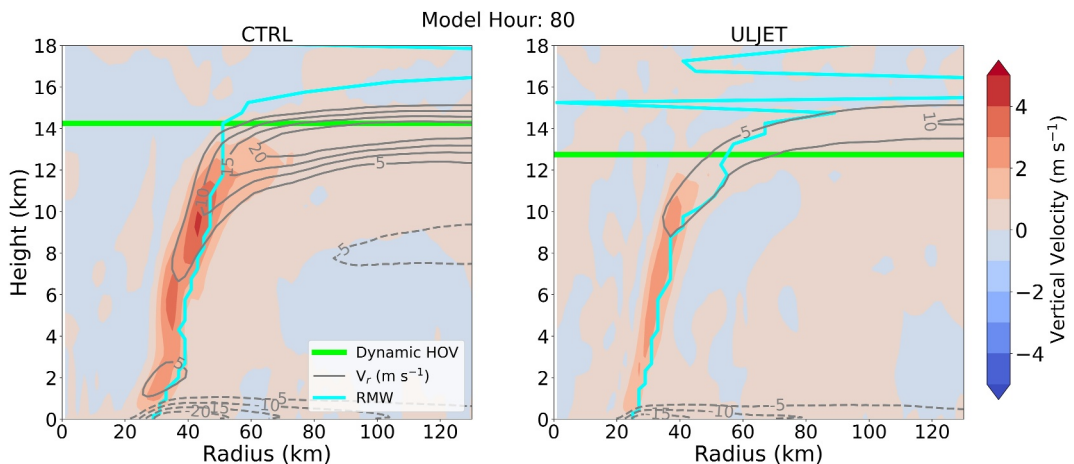


**Figure 14.** Azimuthally-averaged vertical winds (colorbar) and radial winds (gray contours; dashed when negative) at model hour 80 in the (a) control (CTRL) and (b) upper-level jet (ULJET) simulations. The radius of maximum winds (RMW; cyan contour) and dynamic HOV (green line) are given for each.

Smith and Montgomery (2015), solely hydrostatic arguments regarding the upper-level warm core and its influence on  $P_{\min}$  are an insufficient explanation of TC intensification. The complex and interconnected nature of the TC implies processes in other regions, such as the boundary layer, are important as well. Ample focus has been given to the primary tangential circulation in this study, but the secondary circulation, composed of radial and vertical wind components, is a critical component of TC intensification. More detailed analysis of the CTRL and ULJET simulations at hour 80, where their intensities diverge, show the more expansive vertical development in CTRL is associated with a stronger secondary circulation (Figure 14). A lower  $P_{\min}$  (Figure 11b) beneath the TC warm core is accompanied by a stronger radial pressure gradient and supergradient inflow in the boundary layer, capable of importing angular momentum to spin up the maximum winds in the TC. Stronger vertical motion in the convective eyewall region can also vertically advect angular momentum upward aiding in spinup of the vortex above in the free troposphere. This favorable pairing of upper-level vortex development, tracked via the DHOV metric, and a strong secondary circulation is likely important to the continuation of RI to a greater steady-state intensity in the simulated TC in CTRL as compared to ULJET.

## 5. Discussion

Changes to the axisymmetric azimuthally-averaged vertical structure of the vortex wind field are important during TC intensification. The DHOV metric utilized in this study serves as a useful proxy for diagnosing vertical wind field structure in TCs throughout their lifecycle. Analysis of the observational data set utilized in D23 indicates this metric is sensitive to environmental VWS with all observed “short” DHOV values being indicative of tilted vortices. The relationship between DHOV and tilt in observed TCs suggests the aircraft data analyzed in Fitzpatrick (1995) may have contained some of the earliest observational clues of the link between vortex tilt and intensification. Numerical model simulations add greater context to this DHOV-VWS relationship. VWS is known to cause differential advection of the low- and mid-level centers of circulation which tilts the vortex downshear (DeMaria, 1996). The impact of tilt on DHOV is apparent early in the modeled WRF ensemble TCs, which exhibit large magnitudes of tilt and corresponding low values of DHOV during the pre-alignment phase. As the tilt magnitude begins to decrease, there is a large jump in DHOV to exclusively higher values which are maintained as the vortex continues to become more aligned and rapidly intensify (Figure 6).

Alignment in this study is defined as the model hour in which this DHOV jump occurs. The DHOV jump is a key characteristic of the active alignment phase. Although vortex tilt lowers considerably in the time surrounding this period, it remains present but decreasing over the  $\sim 20$  hr following the DHOV-defined alignment time. The onset of RI occurs during the latter times of this period between the DHOV jump and the elimination of tilt as it reduces to near zero. The jump in DHOV preceding RI onset suggests the DHOV jump is a necessary, but insufficient, condition for RI in an initially tilted vortex. The final stages of tilt reduction being concurrent with RI onset is consistent with H. Chen and Gopalakrishnan (2015), who show reduction of vortex tilt continues in the early

stages of RI in the presence of VWS as a consequence of it rather than a precursor. In their simulation of Hurricane Earl (2010) which underwent RI in VWS, tilt reduces from moderate values to much lower ones similar to those found in the ensemble near the DHOV-defined alignment time. The results indicate TC vortex alignment in VWS is likely not a discrete moment as defined here for simplicity, but more of a continuum. The alignment process observed in the WRF ensembles begins with a dramatic improvement of the coherence of the axisymmetric projection of the tangential wind field with respect to height, followed by an increase of the upper-level warm core temperature perturbation at RI onset, which grows rapidly as RI continues.

Analysis of key model times in a representative ensemble member show negative perturbation temperatures at the storm center near 12-km altitude at hour 0, when the DHOV jump occurs, suggesting the increase in upper-level tangential winds during alignment precedes the development of a strong upper-level warm core perturbation temperature maximum (Figure 8). After the initial DHOV jump, a small decline and subsequent growth of DHOV in concert with the strengthening upper-level warm core proceeds in accordance with thermal wind balance in this baroclinic upper-level region of the model TCs. This behavior at the end of the active alignment phase pre-conditions the TC structure for the vertical growth phase of RI that follows. The DHOV jump may be an early indicator of a sheared TC obtaining the vertical structure necessary to develop an upper-level component of its warm core and rapidly align during the initial stages of RI. The DHOV jump is more accurately referred to as “adequate alignment” for TC intensification versus a total reduction of vortex tilt. Deep atmospheric convection is an essential component of TC intensification which is a more efficient agent of the process when located in the inner-core and preferentially occurring within the RMW (Rogers et al., 2013) in the region of high inertial stability (Schubert & Hack, 1982). An analysis of convective characteristics in observed TCs showed deep convection is preferentially located near the mid-level center (Fischer et al., 2024). The movement of the mid-level center into the vicinity of the low-level center produces the DHOV jump and also signals the arrival of deep convection to the TC inner core, which is important to facilitating intensification. Nam et al. (2023) analyzed convective behavior in a larger set of WRF ensembles including the one used here and noted deep convection near the mid-level center organizing near the low-level center as vortex tilt decreases.

Once the adequate alignment condition is met, a developing upper-level circulation and associated warm core are important features in the sheared ensemble simulations as tilt finishes decreasing and RI ensues. The CM1 simulations attempt to isolate the importance of upper-level development to RI during the vertical growth phase of intensification in idealized TCs by using environmental VWS to hinder it via a concentrated upper-level jet. Finocchio et al. (2016) varied both the height of the maximum shear magnitude and the depth of the VWS layer in idealized modeling experiments and found low-level VWS is more effective at tilting the vortex and VWS concentrated in shallow layers are less favorable to TC intensification. Fu et al. (2019) found that concentrated VWS higher in the troposphere in numerical model simulations proved most effective at ventilating the upper-level warm core through dilution of the high-entropy air by an influx of low-entropy air. The simulated TC in ULJET behaved in a manner consistent with the results of these previous studies, although the upper-level jet used here is concentrated in higher atmospheric levels than those tested in the studies previously mentioned. The upper-level jet proved effective at disrupting upper-level TC vortex development, but the absence of lower-level VWS allowed the modeled TC to maintain alignment of the low- and mid-level centers throughout intensification in both CM1 simulations. The duration of RI and peak steady-state intensities reached in CTRL and ULJET after their RI episodes are different with the RI process in ULJET ending at a lesser intensity, resulting in a TC that is still formidable, but considerably weaker than its counterpart in CTRL. Averaging tangential winds and warm core temperature perturbations over vertical layers identified differences in axisymmetric vortex structure located in the upper levels of the vortex from 12- to 16-km altitude (Figure 13). A brief weakening of tangential winds and warm core perturbation temperatures in the upper levels is concurrent with the cessation of RI in ULJET and divergence of intensity between CTRL and ULJET. These declines and associated lesser DHOV and intensity in ULJET show that in these simulated TCs, establishing a coherent vortex structure that extends into the highest levels of the troposphere is an important feature in CTRL, which continues RI and achieves a more extreme intensity. Comparison of the secondary circulations in the modeled TCs as their intensities diverged (Figure 14), helps to link the differences in vertical vortex structure to important intensification processes in other regions of the TC.

The weaker upper-level winds and warming in ULJET as compared to CTRL being most prominent from 14- to 16-km altitude lends credence to the importance of the UTLS warm core and cyclonic wind field present in modeled (Ohno & Satoh, 2015; H. Chen & Zhang, 2013) and observed (Duran & Molinari, 2018) TCs of extreme

intensity. Finocchio and Rios-Berrios (2021) exposed modeled TCs to increasing environmental VWS at different stages of intensification. The strongest TCs exposed to VWS near peak intensity resisted low- to mid-level vortex tilt, but rapidly weakened to steady-state intensities similar to the steady-state  $P_{min}$  value attained by the TC in ULJET. The weakening of these strong simulated TCs may be due in part to VWS ventilation of the UTLS warm core, similar to that proposed by Frank and Ritchie (2001), in which VWS results in loss of the warm core at upper-levels and rising  $P_{min}$  at the surface. The results presented here, although idealized, suggest that TC intensity and intensification have a strong connection to processes which increase the vertical extent of the TC vortex. Intensification of the tangential wind field in the upper-levels is closely tied via thermal wind balance to the development of the upper-level warm core, evidenced by aircraft observations of RI (DesRosiers et al., 2022). The relationship between peak DHOV values and maximum steady-state intensity in the CM1 simulations can be considered with respect to potential intensity (PI) theory. Some derivations of PI theory rely on an estimation of the temperature of the TC outflow in the upper levels of the TC secondary circulation with a colder outflow temperature resulting in a higher calculated PI (Rousseau-Rizzi & Emanuel, 2019). The azimuthally-averaged ULJET vortex structure decays at lower heights than CTRL (Figures 12g and 12h) at steady-state intensity with a concentrated upper-level outflow jet maximized at lower altitude (not shown). In the troposphere, temperatures decrease with height, so a lower outflow jet results in increased outflow temperature, and therefore decreased PI. This agrees in principle with Stern and Nolan (2011) who used a formulation of PI theory with varied SSTs and outflow temperatures to show the decay rate of the tangential wind field should be sensitive to the maximum PI of the TC. Increasing the vertical extent of the warm core should help to lower  $P_{min}$  through hydrostatic arguments, but the additional consideration of PI theory relates the height-intensity connection in TCs to the kinematics of the wind field via the height of the outflow in the secondary circulation.

Both modeling experiments indicate environmental VWS is an important modulator of TC vertical structure evaluated through the azimuthally-averaged lens of DHOV. Different profiles of VWS correspond with different trajectories of DHOV during intensification. VWS present in the lower levels of the atmosphere in the WRF ensemble resulted in long periods of vortex tilt and low DHOV values. During the active alignment phase, DHOV values quickly jump upward followed by a brief decrease and then continued growth during RI. In the CM1 simulations, the vortex remains aligned in the low- to mid-levels where VWS is absent and DHOV continually increases from its starting value during RI at varied rates of increase. The lack of a noticeable jump and decline in DHOV in the CM1 simulations raises the question if this behavior is unique to alignment processes in TCs tilted by VWS. However, the experiments must be compared with some caution as there key differences between the simulation sets. Different choices in parameterization schemes mentioned in the methods are important, but a crucial difference from the WRF ensemble to the CM1 simulations is the inclusion of radiation. Radiation introduces cloud-radiation interactions which are shown to speed up TC development and are likely important to RI as well (Ruppert Jr. et al., 2020). Upper-level TC structure is also sensitive to radiative tendencies (Trabing et al., 2019) which may partially explain the discrepancy between peak DHOV values in the WRF ensemble and CM1 control despite similar peak intensities. Vertical resolution differences could also play a role with 18 additional vertical levels and a model top altitude that is 5 km higher than the WRF ensembles in the CM1 simulations. The model VWS profiles are also sustained with uniformity for long periods of time, which is unlikely to occur in the real atmosphere where VWS varies on shorter timescales (Rios-Berrios & Torn, 2017).

## 6. Conclusions

As tropical cyclones (TCs) intensify, changes in the kinematic and thermal structure of the middle, and especially upper, levels of the troposphere are associated with development of a deep axisymmetric vortex. The work here seeks to build on findings of DesRosiers et al. (2023), referred to as D23, in which all observed TCs possessed deep vertical vortex structure prior to RI. Vertical structure of the vortex wind field is evaluated with the dynamic height of the vortex (DHOV) metric, which is defined as the height at which the azimuthally-averaged tangential wind at the radius of maximum wind (RMW) decays to 40% of its maximum azimuthally-averaged value at 2-km altitude. Environmental vertical wind shear (VWS) can tilt vortices downshear and misalign the mid- and low-level centers, stunting the azimuthally-averaged projection of the tangential wind field. Revisiting the data set of TCs observed with airborne radar utilized in D23 shows that all aligned TCs with minimal vortex tilt, regardless of their intensity at analysis time, exhibit DHOV values  $\geq 10$  km, indicative of the deep vertical vortex structure required for RI. All observed TCs with “short” DHOV values were tilted vortices with their vertical misalignment resulting in weak tangential winds in the middle and upper levels of the troposphere in the azimuthal-average

taken about the low-level circulation center. The absence of low DHOV values in all aligned TCs suggests that “short” TCs of tropical storm intensity or greater may not exist, and vertical alignment is all that is required for a TC to qualify as “tall,” or adequately aligned, using DHOV. Given the analysis presented here is limited to a filtered subset of observations and two sets of idealized model simulations, further work is needed to test if this finding applies more broadly to scenarios not considered in this study. In aligned TCs, observed DHOV values trend upward with intensity, indicating that continued vertical growth of the vortex is an important structural change during TC intensification.

Using DHOV, the evolution of vertical vortex structure in the presence of moderate VWS is explored in numerical model simulations. In the WRF ensemble simulations of TCs developing in moderate shear, a DHOV jump is assigned as the alignment time. The jump is associated with existing rotation about the mid-level center approaching the low-level center, allowing for stronger tangential winds at greater heights when azimuthally-averaged about the low-level center. In the ~20 hr following the DHOV-jump-defined alignment time, there is a subsequent decrease in DHOV associated with initial growth of a warm core perturbation temperature higher in the troposphere. RI onset occurs after the DHOV jump, is concurrent with the increase in upper-level warm core perturbation temperatures, and happens prior to the reduction of vortex tilt to near-zero values. The timing suggests vortex alignment and RI onset are not discrete and simultaneous events, but rather part of a continuous process which may be tracked relative to changes in the azimuthally-averaged tangential winds. Furthermore, “adequate alignment” of the low- and mid-level centers, signaled by sustained DHOV greater than or equal to 10 km, is found to be a necessary condition for RI and a key step in the TC intensification process in moderate VWS. Continued DHOV growth during RI proceeds in concert with rapid strengthening of the upper-level warm core in the simulated TCs during the vertical growth stage, indicating the importance of upper-level vortex development during RI. Therefore, DHOV continuously provides useful diagnostic information about TC structure and intensity change during the pre-alignment, active alignment, and vertical growth phases of intensification in VWS described here.

The sensitivity of the RI process to development of the upper-level warm core is investigated in CM1 simulations in which a control (CTRL) TC is allowed to develop in quiescent flow while another TC evolves in a parallel environment differentiated only by an upper-level jet (ULJET) of moderate VWS. Both simulations begin RI, but the RI period concludes sooner in ULJET, resulting in a lesser steady-state TC intensity and a lower peak DHOV value than in the CTRL simulation. Higher DHOV in CTRL was also associated with a more robust secondary circulation as compared to that of ULJET. Despite both TCs maintaining vertical alignment of the low- and mid-level centers, the upper-level jet prevents formation of a strong upper-level warm core and effectively serves to cap the vertical development of the vortex. In the aligned RI of CTRL, the jump and decrease behavior of DHOV in the WRF ensemble TCs in moderate VWS is noticeably absent. Differences in the evolution may be indicative of different RI pathways with respect to vertical structure in different VWS environments, but several key differences in model configuration likely contribute as well. Calculation of azimuthally-averaged winds and perturbation temperatures in both CM1 experiments confirm their evolution in most lower and middle vertical levels of the TCs are similar and the biggest differences are present in the upper levels. The greatest differences were between 12 and 16-km altitude where CTRL developed localized perturbation temperature maxima while the thermal structure of ULJET decayed rapidly with height. Differences at these altitudes as well as differences in peak steady-state intensity suggest the presence, or lack, of a component of the warm core at the interface between the upper-troposphere and lower-stratosphere (UTLS) may be important to extending the duration of RI and setting a ceiling for the peak steady-state intensity a TC can achieve. Vertical structure seems to be primarily related to the profile of environmental VWS. Although vortex tilt explains most of the reduction of DHOV in observed cases and the WRF ensemble, the CM1 results suggest that upper-level VWS may be capable of limiting the vertical extent of TCs regardless of alignment in the lower and middle levels of the troposphere.

Through the lens of potential intensity (PI) theory, DHOV and TC intensity are linked via the relationship between the vertical location of TC outflow and the outflow temperature. Lower outflow temperatures in a taller TC create a greater temperature differential between the outflow layer and the surface, and therefore a stronger PI. Upper-level structural changes in TCs are likely sensitive to choices made in horizontal and vertical resolution as well as radiation and other parameterization schemes (Duran & Molinari, 2019). Sensitivity tests with these choices and their impacts on development of the upper-level vortex would be a useful effort in future work. The inability to develop a UTLS warm core in ULJET motivates numerical modeling experiments to discern just how vulnerable this feature, which exists in a region of weak inertial stability, is to radial ventilation by varied

magnitudes of upper-level VWS. The mechanisms by which the warm core in the upper levels of a TC intensifies may differ from lower levels of the troposphere. Understanding these potential differences could help discern how the TC intensification process may change throughout an RI event. Agreement of the DHOV analysis conducted here with the findings of several past studies of TC vertical structure and intensity change described in the discussion section indicate DHOV is a useful vertical structural metric for subsequent work on the topic. The results of this study also help to explain the observed relationship between DHOV and intensity change found in D23. Continued investigation of internal processes and environmental conditions which modulate vertical vortex structure and DHOV should improve our understanding of RI, providing the field with additional knowledge with which to improve TC intensity forecasts.

## Data Availability Statement

Calculated observed DHOV metrics from TC-RADAR (version v3k), the time series of calculated values for the WRF ensemble, and input files necessary to reproduce the CM1 simulations are available on Figshare (DesRosiers & Bell, 2024). Information regarding access to TC-RADAR is included in Fischer et al. (2022).

## Acknowledgments

We appreciate assistance from Chelsea Nam while working with the WRF ensemble simulations. Numerous conversations with scientists in the Colorado State University Department of Atmospheric Science and Cooperative Institute for Research in the Atmosphere (CIRA) helped shape the analysis presented here. The authors thank Mark DeMaria and two anonymous reviewers for helpful and insightful feedback during peer review. This research is supported by Office of Naval Research Award N000142012069.

## References

- Aircraft Operations Center. (2016). *Tropical cyclone operations: Challenges in 2015; New products and services planned for 2016 and 2017*. NOAA Office of Marine and Aviation Operations. Retrieved from <https://www.ofcm.gov/meetings/TCORF/ihc16/2016presentations.html>
- Allard, J. J., Tang, B. H., Corbosiero, K. L., & Bryan, G. H. (2021). Combined effects of midlevel dry air and vertical wind shear on tropical cyclone development. Part I: Downdraft ventilation. *Journal of the Atmospheric Sciences*, 78(3), 763–782. <https://doi.org/10.1175/JAS-D-20-0054.1>
- Bryan, G. H., & Fritsch, M. J. (2002). A benchmark simulation for moist nonhydrostatic numerical models. *Monthly Weather Review*, 130(12), 2917–2928. [https://doi.org/10.1175/1520-0493\(2002\)130\(2917:ABSFNM\)2.0.CO;2](https://doi.org/10.1175/1520-0493(2002)130(2917:ABSFNM)2.0.CO;2)
- Bryan, G. H., & Rotunno, R. (2009). The maximum intensity of tropical cyclones in axisymmetric numerical model simulations. *Monthly Weather Review*, 137(6), 1770–1789. <https://doi.org/10.1175/2008MWR2709.1>
- Cangialosi, J. P., Blake, E., DeMaria, M., Penny, A., Latto, A., Rappaport, E., & Tallapragada, V. (2020). Recent progress in tropical cyclone intensity forecasting at the National Hurricane Center. *Weather and Forecasting*, 35(5), 1913–1922. <https://doi.org/10.1175/WAF-D-20-0059.1>
- Chen, H., & Gopalakrishnan, S. G. (2015). A study on the asymmetric rapid intensification of Hurricane Earl (2010) using the HWRF system. *Journal of the Atmospheric Sciences*, 72(2), 531–550. <https://doi.org/10.1175/JAS-D-14-0097.1>
- Chen, H., & Zhang, D.-L. (2013). On the rapid intensification of Hurricane Wilma (2005). Part II: Convective bursts and the upper-level warm core. *Journal of the Atmospheric Sciences*, 70(1), 146–162. <https://doi.org/10.1175/JAS-D-12-062.1>
- Chen, X., Rozoff, C. M., Rogers, R. F., Corbosiero, K. L., Tao, D., Gu, J.-F., et al. (2023). Research advances on internal processes affecting tropical cyclone intensity change from 2018–2022. *Tropical Cyclone Research and Review*, 12(1), 10–29. <https://doi.org/10.1016/j.tcr.2023.05.001>
- Choudhury, D., & Das, S. (2017). The sensitivity to the microphysical schemes on the skill of forecasting the track and intensity of tropical cyclones using WRF-ARW model. *Journal of Earth System Science*, 126, 1–10. <https://doi.org/10.1007/s12040-017-0830-2>
- DeMaria, M. (1996). The effect of vertical shear on tropical cyclone intensity change. *Journal of the Atmospheric Sciences*, 53(14), 2076–2088. [https://doi.org/10.1175/1520-0469\(1996\)053\(2076:TEOVSO\)2.0.CO;2](https://doi.org/10.1175/1520-0469(1996)053(2076:TEOVSO)2.0.CO;2)
- DesRosiers, A. J., & Bell, M. M. (2024). Dynamic vortex height evolution during RI dataset. Published: 2024-11-24. Retrieved from <https://figshare.com/s/b95d4351919ef2ff056a>
- DesRosiers, A. J., Bell, M. M., & Cha, T.-Y. (2022). Vertical vortex development in Hurricane Michael (2018) during rapid intensification. *Monthly Weather Review*, 150(1), 99–114. <https://doi.org/10.1175/MWR-D-21-0098.1>
- DesRosiers, A. J., Bell, M. M., Klotzbach, P. J., Fischer, M. S., & Reasor, P. D. (2023). Observed relationships between tropical cyclone vortex height, intensity, and intensification rate. *Geophysical Research Letters*, 50(8), e2022GL101877. <https://doi.org/10.1029/2022GL101877>
- Dunion, J. P. (2011). Rewriting the climatology of the tropical north Atlantic and Caribbean Sea atmosphere. *Journal of Climate*, 24(3), 893–908. <https://doi.org/10.1175/2010JCLI3496.1>
- Dunion, J. P., & Marron, C. S. (2008). A reexamination of the Jordan mean tropical sounding based on awareness of the Saharan air layer: Results from 2002. *Journal of Climate*, 21(20), 5242–5253. <https://doi.org/10.1175/2008JCLI1868.1>
- Duran, P., & Molinari, J. (2018). Dramatic inner-core tropopause variability during the rapid intensification of Hurricane Patricia (2015). *Monthly Weather Review*, 146(1), 119–134. <https://doi.org/10.1175/MWR-D-17-0218.1>
- Duran, P., & Molinari, J. (2019). Tropopause evolution in a rapidly intensifying tropical cyclone: A static stability budget analysis in an idealized axisymmetric framework. *Monthly Weather Review*, 76(1), 209–229. <https://doi.org/10.1175/JAS-D-18-0097.1>
- Finocchio, P. M., Majumdar, S. J., Nolan, D. S., & Iskandarani, M. (2016). Idealized tropical cyclone responses to the height and depth of environmental vertical wind shear. *Monthly Weather Review*, 144(6), 2155–2175. <https://doi.org/10.1175/MWR-D-15-0320.1>
- Finocchio, P. M., & Rios-Berrios, R. (2021). The intensity- and size-dependent response of tropical cyclones to increasing vertical wind shear. *Journal of the Atmospheric Sciences*, 78, 3673–3690. <https://doi.org/10.1175/JAS-D-21-0126.1>
- Fischer, M. S., Reasor, P. D., Rogers, R. F., & Gamache, J. F. (2022). An analysis of tropical cyclone vortex and convective characteristics in relation to storm intensity using a novel airborne Doppler radar database. *Monthly Weather Review*, 150(9), 2255–2278. <https://doi.org/10.1175/MWR-D-21-0223.1>
- Fischer, M. S., Rogers, R. F., Reasor, P. D., & Dunion, J. P. (2024). An observational analysis of the relationship between tropical cyclone vortex tilt, precipitation structure, and intensity change. *Monthly Weather Review*, 152(1), 203–225. <https://doi.org/10.1175/MWR-D-23-0089.1>
- Fitzpatrick, P. J. (1995). Understanding and forecasting tropical cyclone intensity change. PhD dissertation. Colorado State University, Department of Atmospheric Science. Retrieved from <https://proquest.com/docview/304182853/abstract/6607DA52E8EE4EF9PQ/1?accountid=10223&sourcetype=Dissertations%20&%20Theses>

- Frank, W. M., & Ritchie, E. A. (2001). Effects of vertical wind shear on the intensity and structure of numerically simulated hurricanes. *Monthly Weather Review*, 129(9), 2249–2269. [https://doi.org/10.1175/1520-0493\(2001\)129\(2249:EOVWSO\)2.0.CO;2](https://doi.org/10.1175/1520-0493(2001)129(2249:EOVWSO)2.0.CO;2)
- Fu, H., Riemer, M., & Li, Q. (2019). Effect of unidirectional vertical wind shear on tropical cyclone intensity change—Lower-layer shear versus upper-layer shear. *Journal of Geophysical Research: Atmospheres*, 124, 6265–6282. <https://doi.org/10.1029/2019JD030586>
- Hendricks, E. A., Peng, M. S., Fu, B., & Li, T. (2010). Quantifying environmental control on tropical cyclone intensity change. *Monthly Weather Review*, 138(8), 3243–3271. <https://doi.org/10.1175/2010MWR3185.1>
- Hong, S.-Y., Dudhia, J., & Chen, S.-H. (2004). A revised approach to ice microphysical processes for the bulk parameterization of clouds and precipitation. *Monthly Weather Review*, 132(1), 103–120. [https://doi.org/10.1175/1520-0493\(2004\)132\(0103:ARATIM\)2.0.CO;2](https://doi.org/10.1175/1520-0493(2004)132(0103:ARATIM)2.0.CO;2)
- Hong, S.-Y., Noh, Y., & Dudhia, J. (2006). A new vertical diffusion package with an explicit treatment of entrainment processes. *Monthly Weather Review*, 134(9), 2318–2341. <https://doi.org/10.1175/MWR3199.1>
- Kaplan, J., & DeMaria, M. (2003). Large-scale characteristics of rapidly intensifying tropical cyclones in the North Atlantic basin. *Weather and Forecasting*, 18(6), 1093–1108. [https://doi.org/10.1175/1520-0434\(2003\)018\(1093:LCORIT\)2.0.CO;2](https://doi.org/10.1175/1520-0434(2003)018(1093:LCORIT)2.0.CO;2)
- Kaplan, J., DeMaria, M., & Knaff, J. A. (2010). A revised tropical cyclone rapid intensification index for the Atlantic and Eastern North Pacific basins. *Weather and Forecasting*, 25(1), 220–241. <https://doi.org/10.1175/2009WAF2222280.1>
- Klotzbach, P. J., Chavas, D. R., Bell, M. M., Bowen, S. G., Gibney, E. J., & Schreck, C. J., III. (2022). Characterizing continental US hurricane risk: Which intensity metric is best? *Journal of Geophysical Research: Atmospheres*, 127(18), e2022JD037030. <https://doi.org/10.1029/2022JD037030>
- Martinez, J., Bell, M. M., Rogers, R., & Doyle, J. D. (2019). Axisymmetric potential vorticity evolution of Hurricane Patricia (2015). *Journal of the Atmospheric Sciences*, 76(7), 2043–2063. <https://doi.org/10.1175/JAS-D-18-0373.1>
- Martinez, J., Davis, C. A., & Bell, M. M. (2022). Eyewall asymmetries and their contributions to the intensification of an idealized tropical cyclone translating in uniform flow. *Journal of the Atmospheric Sciences*, 79(9), 2471–2491. <https://doi.org/10.1175/JAS-D-21-0302.1>
- Nam, C. C., Bell, M. M., & Tao, D. (2023). Bifurcation points for tropical cyclone genesis and intensification in sheared and dry environments. *Journal of the Atmospheric Sciences*, 80(9), 2239–2259. <https://doi.org/10.1175/JAS-D-22-0100.1>
- Nguyen, L. T., Molinari, J., & Thomas, D. (2014). Evaluation of tropical cyclone center identification methods in numerical models. *Monthly Weather Review*, 142(11), 4326–4339. <https://doi.org/10.1175/MWR-D-14-00044.1>
- Nolan, D. S. (2011). Evaluating environmental favorability for tropical cyclone development with the method of point-downscaling. *Journal of Advances in Modeling Earth Systems*, 3(8), M08001. <https://doi.org/10.1029/2011MS000063>
- Ohno, T., & Satoh, M. (2015). On the warm core of a tropical cyclone formed near the tropopause. *Journal of the Atmospheric Sciences*, 72(2), 551–571. <https://doi.org/10.1175/JAS-D-14-0078.1>
- Onderlinde, M. J., & Nolan, D. S. (2017). The tropical cyclone response to changing wind shear using the method of time-varying point-downscaling. *Journal of Advances in Modeling Earth Systems*, 9(2), 908–931. <https://doi.org/10.1002/2016MS000796>
- Peng, K., & Fang, J. (2021). Effect of the initial vortex vertical structure on early development of an axisymmetric tropical cyclone. *Journal of Geophysical Research*, 126(4), e2020JD033697. <https://doi.org/10.1029/2020JD033697>
- Rios-Berrios, R., Davis, C. A., & Torn, R. D. (2018). A hypothesis for the intensification of tropical cyclones under moderate vertical wind shear. *Journal of the Atmospheric Sciences*, 75(12), 4149–4173. <https://doi.org/10.1175/JAS-D-18-0070.1>
- Rios-Berrios, R., Finocchio, P. M., Alland, J. J., Chen, X., Fischer, M. S., Stevenson, S. N., & Tao, D. (2024). A review of the interactions between tropical cyclones and environmental vertical wind shear. *Journal of the Atmospheric Sciences*, 81(4), 713–741. <https://doi.org/10.1175/JAS-D-23-0022.1>
- Rios-Berrios, R., & Torn, R. D. (2017). Climatological analysis of tropical cyclone intensity changes under moderate vertical wind shear. *Monthly Weather Review*, 145(5), 1717–1738. <https://doi.org/10.1175/MWR-D-16-0350.1>
- Rogers, R. F., Aberson, S., Bell, M. M., Cecil, D. J., Doyle, J. D., Kimberlain, T. B., et al. (2017). Rewriting the tropical record books: The extraordinary intensification of Hurricane Patricia (2015). *Bulletin of the American Meteorological Society*, 98(10), 2091–2112. <https://doi.org/10.1175/BAMS-D-16-0039.1>
- Rogers, R. F., Reasor, P., & Lorsolo, S. (2013). Airborne Doppler observations of the inner-core structural differences between intensifying and steady-state tropical cyclones. *Monthly Weather Review*, 141(9), 2970–2991. <https://doi.org/10.1175/MWR-D-12-00357.1>
- Rousseau-Rizzi, R., & Emanuel, K. (2019). An evaluation of hurricane superintensity in axisymmetric numerical models. *Journal of the Atmospheric Sciences*, 76(6), 1697–1708. <https://doi.org/10.1175/JAS-D-18-0238.1>
- Ruppert Jr, J. H., Wing, A. A., Tang, X., & Duran, E. L. (2020). The critical role of cloud-infrared radiation feedback in tropical cyclone development. *Proceedings of the National Academy of Sciences*, 117(45), 27884–27892. <https://doi.org/10.1073/pnas.2013584117>
- Schubert, W. H., & Hack, J. J. (1982). Inertial stability and tropical cyclone development. *Journal of the Atmospheric Sciences*, 39(8), 1687–1697. [https://doi.org/10.1175/1520-0469\(1982\)039\(1687:ISATCD\)2.0.CO;2](https://doi.org/10.1175/1520-0469(1982)039(1687:ISATCD)2.0.CO;2)
- Skamarock, W. C., Klemp, J. B., Dudhia, J., Gill, D. O., Barker, D. M., Duda, M. G., et al. (2008). A description of the advanced research WRF version 3. *NCAR Technical Note*, 475, 113.
- Smith, R. K., & Montgomery, M. T. (2015). Toward clarity on understanding tropical cyclone intensification. *Journal of the Atmospheric Sciences*, 72(8), 3020–3031. <https://doi.org/10.1175/JAS-D-15-0017.1>
- Stern, D. P., Brisbois, J. R., & Nolan, D. S. (2014). An expanded dataset of hurricane eyewall sizes and slopes. *Journal of the Atmospheric Sciences*, 71(7), 2747–2762. <https://doi.org/10.1175/JAS-D-13-0302.1>
- Stern, D. P., & Nolan, D. S. (2011). On the vertical decay rate of the maximum tangential winds in tropical cyclones. *Journal of the Atmospheric Sciences*, 68(9), 2073–2094. <https://doi.org/10.1175/2011JAS3682.1>
- Tao, D., & Zhang, F. (2014). Effect of environmental shear, sea-surface temperature, and ambient moisture on the formation and predictability of tropical cyclones: An ensemble-mean perspective. *Journal of Advances in Modeling Earth Systems*, 6(2), 384–404. <https://doi.org/10.1002/2014MS000314>
- Thompson, G., Rasmussen, R. M., & Manning, K. (2004). Explicit forecasts of winter precipitation using an improved bulk microphysics scheme. Part I: Description and sensitivity analysis. *Monthly Weather Review*, 132(2), 519–542. [https://doi.org/10.1175/1520-0493\(2004\)132\(0519:EFPWPU\)2.0.CO;2](https://doi.org/10.1175/1520-0493(2004)132(0519:EFPWPU)2.0.CO;2)
- Trabing, B. C., & Bell, M. M. (2020). Understanding error distributions of hurricane intensity forecasts during rapid intensity changes. *Weather and Forecasting*, 35(6), 2219–2234. <https://doi.org/10.1175/WAF-D-19-0253.1>
- Trabing, B. C., & Bell, M. M. (2021). The sensitivity of eyewall replacement cycles to shortwave radiation. *Journal of Geophysical Research: Atmospheres*, 126(8), e2020JD034016. <https://doi.org/10.1029/2020JD034016>
- Trabing, B. C., Bell, M. M., & Brown, B. R. (2019). Impacts of radiation and upper-tropospheric temperatures on tropical cyclone structure and intensity. *Journal of the Atmospheric Sciences*, 76(1), 135–153. <https://doi.org/10.1175/JAS-D-18-0165.1>